## Longitudinal and transverse photophoretic

# 2 force on a homogeneous sphere exerted by a

# 3 zero-order Bessel beam with selective

## 4 polarizations

- 5 YIHENG SUN, 1 JIAJIE WANG, 1, 2 QIANJIANG YU, 1 HAOXIANG WANG, 1 PAUL
- 6 BRIARD, LEONARDO ANDRÉ AMBROSIO<sup>2</sup>, GÉRARD GOUESBET<sup>3</sup>
- 7 School of Physics, Xidian University, Xi'an, 710071, P. R. China.
- 8 <sup>2</sup>. Department of Electrical and Computer Engineering. São Carlos School of Engineering, University of
- 9 São Paulo. 400 Trabalhador são-carlense Ave. 13566-590, São Carlos, SP, Brazil.
- 10 <sup>3</sup> CORIA-UMR 6614 Normandie Université. CNRS-Université et INSA de Rouen. Campus
- 11 Universitaire du Madrillet. 76800, Saint-Etienne du Rouvray, France.
- \*wangjiajie@xidian.edu.cn
- 13 Abstract: The prediction of photophoretic force exerted on an optical absorptive particle in a
- gaseous medium is a challenging problem, since the problems of electromagnetic scattering,
- heat transfer, and gaseous molecule dynamics are involved and coupled with each other. Based
- on the calculation of source function distribution inside a homogeneous sphere excited by a
- 17 zero-order Bessel beam with the aid of generalized Lorenz-Mie theory (GLMT), analytical
- 18 expressions of asymmetry vector, which is a crucial quantity in the calculation of photophoretic
- force, are given using the adjoint boundary value method. Numerical simulations are performed
- to analyze the influences of polarization and half-cone angle of the incident beam, particle size,
- and absorptivity of the particle on the asymmetry vector for both on-axis and off-axis
- 22 illumination. Longitudinal and transverse photophoretic forces on a homogeneous sphere are
- 23 displayed for slip-flow regime of gaseous media. The results give us insights into the working
- 24 mechanism underpinning the development of novel heat-mediated optical manipulation
- 25 techniques, measurement of the refractive index of particles, and others.
- 26 © 2021 Optica Publishing Group

### 27 1. Introduction

- 28 The rapid progress in the precise manipulation of small particles have produced significant
- advances in various fields, including biomedicine, physical chemistry, nanotechnology, etc.
- 30 Among the various approaches used in particle trapping and manipulation, increased attention
- 31 has been given to the optical methods due to their intrinsic advantages, including high
- 32 resolution in space, non-intrusive and high precision in sensing [1]. The conventional optical
- tweezers, proposed by Ashkin in 1970, have been widely applied in various fields that he was
- 34 awarded the Nobel Prize in Physics in 2018 [2]. Conventional optical tweezers based on the
- 35 gradient (non-thermal) forces to trap and manipulate small particles using a tightly focused
- 36 laser beam have certain limitations. For instance, the gradient force is around ~pN level, various
- 37 perturbations from the ambient surroundings influence the trapping efficiency significantly that
- 38 this technique is commonly used in liquid media where various perturbations can be diminished.
- 39 Furthermore, the distance between the high-aperture object lens and the trapped particle is quite
- 40 limited, making difficult the simultaneous implementation of other collaborative measuring
- 41 techniques. Compared to the conventional optical tweezers, the new emerging heat-mediated
- 42 optical manipulation technique based on photophoretic force demonstrates flexible control of
- 43 lossy particles of various shapes, sizes, and compositions in gaseous media. The simple optical
- 44 configurations and long manipulation range of photopheresis-based optical manipulation in
- experiments enable great potential applications to characterize physical and chemical properties

of aerosol particles [3, 4], in combination with other techniques, such as light scattering, Raman spectroscopy, and in realizing three-dimensional images in space known as optical trap displays [5].

Compared to the recent breakthroughs in the experimental line, theoretical analysis of photophoretic forces exerted by a structured laser beam on an absorbing particle is quite challenging and less developed, in particular because it is an interdisciplinary coupled problem involving electromagnetic scattering, thermal dynamics, and gaseous molecule dynamics, and also because most of the previous investigations were motivated by the applications in atmospheric science and astrophysics [6], where a plane wave illumination is always assumed. When an optical absorptive particle is illuminated, a temperature gradient appears on the surface of the particle originating from the non-uniform absorption of radiant energy within the particle. Then, uneven momentum transfer between the particle and the gas molecules on the particle surface results in the photophoretic force, which depends on the properties of particles (shape, size, material), the parameters of gas media (pressure, composition), and the illumination conditions. In the case of a homogeneous sphere illuminated by a plane wave, axial symmetric distributions of the internal field and the heat source function are obtained so that the photophoretic force arising from this kind of longitudinal unbalanced heat absorption in a non-volatile homogeneous lossy sphere is a longitudinal force along the propagation direction of the light. It can be attractive or repulsive, pulling the particle toward or pushing the particle away from the light source, depending on an asymmetry factor J, which imbeds all the information of the uneven absorption of radiation and reflects the heat source distribution in the particle [7, 8]. As far as the axial symmetry of the electromagnetic scattering is preserved, the photophoretic force has only a longitudinal component, for instance, in the case when an axisymmetric particle is illuminated by an axisymmetric beam under on-axis configuration [9-11].

However, the asymmetric factor is extended to a vectorial quantity once axial symmetry in the electromagnetic scattering is lost, which is a more practical case since the particle is in a dynamic motion and not always in the center of the beam. Then a transversal component of the photophoretic force occurs. By developing a method to predict the photophoretic force for non-spherical particles, the asymmetry factor  $J_1$  was extended to a asymmetry vector J by Rohatschek and Zulehner [12], and the photophoretic force was expressed in terms of the asymmetry vector. Some attempts can be found to consider the influence of field profiles of the incident laser beam on the photophoretic force, but approximated methods or numerical methods were used, which lack efficiency, and a full analysis was not covered [13, 14]. The underlying mechanisms of photophoretic force exerted by a structured laser beam, which plays a significant role in the guide of further developments, are not fully understood,.

In recent two years, the photopheresis of cylindrical particles, including a dielectric cylinder [15], a magneto-dielectric cylinder [16], a cylinder near a planar boundary and corners [17, 18], and two parallel cylinders [19], were analyzed by Mitri, where the influences of light sheets with different polarizations and incidence directions were considered. Based on the analysis performed by Mackowski [7] on the photophoretic force of a homogeneous sphere illuminated by a plane wave, Ambrosio [20] extended the investigation to the cases of axisymmetric beams of the first kind of on-axis illumination using the generalized Lorenz-Mie theory, where fundamental Gaussian beam and zero-order Bessel beam were considered as examples. A study of high-order Bessel beams in the on-axis case was then performed to analyze the characteristics of photophoretic force exerted by a hollow beam [21]. Very recently, the calculation of asymmetry vector J of a sphere was extended to the cases of arbitrarily shaped laser beams with arbitrary illumination [22] with the aid of the generalized Lorenz-Mie theory (GLMT), which forms a solid foundation for predicting photophoretic force on a regular-shaped particle in the case of a structured laser beam. In this paper, this method is applied to the case of Bessel

beams illumination with different polarizations. This work is motivated by the results that the trapping efficiency was confirmed to be sensitive in a photophoretic trap where a radially or azimuthally polarized laser beam was used in the experiments [23], which provides additional flexibility to the optical micromanipulation of light-absorbing particles in gaseous media. However, as far as we know, no rigorous quantitative theoretical analysis is available to interpret the influence of polarization on the photophoretic force exerted on an absorbing sphere illuminated by a structured laser field. Thus, Bessel beams of selective polarizations are implemented for both on-axis and off-axis illumination to analyze the influence of polarization and location on the photophoretic force, which casts insights into the physical mechanism of dynamic behavior of a particle trapped in a Bessel beam.

The rest of this paper is organized as follows. In Section 2, brief description of the theoretical prediction of photophoretic forces of a sphere illuminated by a Bessel beam is presented, where numerical-ready mathematical expressions are provided. Detailed simulation results are displayed in Section 3 for the behaviors of asymmetry vector and photophoretic force in different conditions. The influences of particle size, imaginary part of refractive index, half-cone angle, and particle location on the photophoretic force are explored. Section 4 is a conclusion.

#### 2. Photophoretic force and asymmetry vector

 For a homogeneous non-volatile sphere in the gaseous medium illuminated by a plane wave, analytical solutions can be obtained [7] in different conditions depending on the Knudsen number Kn = l/a, where l and a are the mean free path of the gas molecules and the particle size, respectively. On the one hand, in the slip-flow or continuous regime, where the size of the particle is much larger than the mean free path of the gas molecules leading to Kn < 1 or Kn << 1, the photophoretic force is mainly due to the thermal creep around the particle. By applying the boundary conditions, the photophoretic force for a non-volatile sphere in the slip-flow regime is given by Mackowski [7]:

flow regime is given by Mackowski [7]: 
$$F_p = -\frac{4\pi c_s \eta_g^2 I_{\lambda} a}{\rho_g k_s T_0} \frac{1}{(1+3c_m l/a)(1+2c_t l/a+2k_g/k_s)} J_1. \tag{1}$$

where  $c_s$ ,  $c_m$  and  $c_t$  are the momentum exchange coefficient, the thermal slip coefficient and the jump coefficient, respectively.  $T_0$  is the temperature at infinity, which is assumed to be the ambient gas temperature.  $\rho_g$  and  $\eta_g$  are the density and viscosity of the surrounding gaseous medium, respectively.  $I_{\lambda}$  is the intensity of the incident wave.  $k_g$  and  $k_s$  are the thermal conductivity of the gas and that of the particle, respectively. For the special case Kn << 1, Eq. (1) can be approximated by:

129 
$$F_{p} = -\frac{4\pi c_{s} \eta_{g}^{2} I_{\lambda} a}{\rho_{g} T_{0}} \frac{1}{(k_{s} + 2k_{g})} J_{1}. \tag{2}$$

which is the same as that given by Yalamov [9]. For a strong absorbing particle where radiation is absorbed entirely on the illuminated surface, the asymmetry factor  $J_1 = -0.5$ , and Eq. (1) reduced to that given by Reed [24].

On the other hand, if the size of the particle is much smaller than the mean free path of the gas molecules, we have Kn >> 1. Then the kinetic theory of gases is applied to give an analytical solution to the photophoretic force for a non-volatile sphere [7]:

136 
$$F_{p} = -\frac{\pi^{2} \alpha \eta_{g}^{2} I_{\lambda} a}{6 \rho_{v} k_{v} T_{0}} \frac{(a/l)^{2}}{1 + H_{m}} J_{1}.$$
 (3)

137 where

$$H_m = \frac{4\alpha}{15} \frac{k_g}{k_s} \frac{a}{l} \,. \tag{4}$$

where  $\alpha$  is the thermal accommodation coefficient defined as the ratio of the net molecular kinetic energy transfer to the particle to that obtained if all reflected molecules were characterized by a Maxwellian distribution evaluated at the actual local surface temperature.

142 Considering the definition [7]:

143 
$$l = 2\eta_g \left(\frac{\pi M}{8RT_0}\right)^{1/2} \frac{1}{\rho_g}, \quad k_s = \frac{15}{4}\eta_g \frac{R}{M}$$
 (5)

where R is the gas constant, M is the mole mass of the gas. Eq. (3) can be written as:

$$F_p = -\frac{\pi a^3 \alpha p I_{\lambda}}{3(ha + k_s)T_0} J_1. \tag{6}$$

where h is the molecular heat transfer coefficient. Eq.(6) is the same as those given by Zulehner and Rohatschek [12]. For radiation absorbed entirely on the particle surface, where  $J_1 = -0.5$ , then Eq. (6) is the same as that given by Hidy and Brock [25] with  $h = \alpha p\overline{v}/(2T_0)$ .

As shown in Eqs. (1)-(6), in both the slip-flow and the free molecule regimes, the photophoretic forces have the same dependency upon the radiative absorption, which is embodied in the photophoretic asymmetry factor  $J_1$ . The  $J_1$  incorporates the information on the heat distribution which can be found from the heat source function predicted using the classical Lorenz-Mie theory:

$$J_{1} = \frac{3nkx}{2\pi} \int_{0}^{1} t^{3} dt \int_{0}^{2\pi} d\varphi \int_{-1}^{1} B(t, \mu) \mu d\mu.$$
 (7)

where  $x=2\pi a/\lambda$  and  $m_p=n+i\kappa$  are the size parameter and the relative refractive index of the particle, respectively, with  $\lambda$  being the wavelength of the incident laser beam. In addition,  $B=(\mathbf{E}\cdot\mathbf{E}^*)/E_0^2$  is known as the normalized source function [26],  $\mathbf{E}$  is the electric component of the internal field inside the particle and  $E_0$  its corresponding field strength. The t=r/a is a dimensionless variable, and  $\mu=\cos\theta$ .

In the case of a homogeneous sphere illuminated by a plane wave, axial symmetric distributions of the internal field and the heat source function are obtained, and the asymmetry factor  $J_1$  is a scalar quantity. The photophoretic force arising from this kind of longitudinal unbalanced heat absorption in a non-volatile homogeneous lossy sphere is a longitudinal force along the propagation direction of the light. However, the scalar asymmetric factor  $J_1$  is extended to a vector J once the axial symmetry in the electromagnetic scattering is no more preserved, and a transverse component of the photophoretic force occurs [16-18, 22].

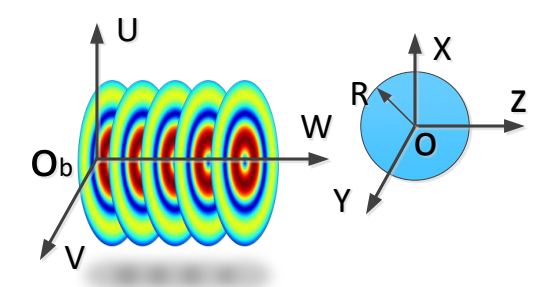


Fig. 1. Illustration of a homogeneous sphere illuminated by an off-axis Bessel beam

154

155

156

157158

159

160

161

162163

164

165

166

In the case of a homogeneous sphere illuminated by an off-axis Bessel beam, as illustrated in Fig. 1, the photophoretic force can be expressed in terms of the asymmetric vector as:

$$\mathbf{F}_{\mathrm{ph}} = -C_{K_n} \mathbf{J} \,. \tag{8}$$

where  $C_{Kn}$  is a constant value depends on the ambient atmosphere condition and parameters of the particle, and **J** is the asymmetric vector:

174 
$$\mathbf{J} = J_{x}\hat{x} + J_{y}\hat{y} + J_{z}\hat{z} . \tag{9}$$

175 where [22]

185

176 
$$J_{\left\{x\right\}}^{x} = \frac{6nk}{|M|^{2}} \left\{ \operatorname{Re} \right\} \sum_{n=1}^{\infty} \left[ A_{n}^{m} (S_{n}^{*} + \frac{n+1}{M} R_{n+1}) + B_{n}^{m} (-S_{n} + \frac{n+1}{M} R_{n}) + i C_{n}^{m} S_{n} \right].$$
 (10)

177 
$$J_{z} = -\frac{12nk}{|M|^{2} x^{3}} \operatorname{Im} \sum_{n=1}^{\infty} \sum_{m=-n}^{n} \left[ D_{n}^{m} (S_{n}^{*} + \frac{n+1}{M} R_{n+1}) + E_{n}^{m} (-S_{n} + \frac{n+1}{M} R_{n}) + i F_{n}^{m} S_{n} \right].$$
 (11)

178
$$A_{n}^{m} = \frac{1}{(n+1)^{2}} \left\{ \sum_{m=0}^{n-1} d_{n} d_{n+1}^{*} g_{n+1,TM}^{m,*} g_{n,TM}^{m+1} \frac{(n+|m|+1)!}{(n-|m|-1)!} + \sum_{m=0}^{n} d_{n}^{*} d_{n+1} g_{n,TM}^{m,*} g_{n+1,TM}^{m+1} \frac{(n+|m|+2)!}{(n-|m|)!} - \sum_{m=-n}^{-1} d_{n} d_{n+1}^{*} g_{n+1,TM}^{m,*} g_{n+1,TM}^{m+1} \frac{(n+|m|+1)!}{(n-|m|+1)!} - \sum_{m=-n}^{-1} d_{n}^{*} d_{n+1} g_{n,TM}^{m,*} g_{n+1,TM}^{m+1} \frac{(n+|m|+2)!}{(n-|m|)!} \right\}$$

$$(12)$$

$$B_{n}^{m} = \frac{1}{(n+1)^{2}} \left\{ \sum_{m=0}^{n-1} c_{n} c_{n+1}^{*} g_{n+1,TE}^{m,*} g_{n,TE}^{m+1} \frac{(n+|m|+1)!}{(n-|m|-1)!} + \sum_{m=0}^{n} c_{n}^{*} c_{n+1} g_{n,TE}^{m,*} g_{n+1,TE}^{m+1} \frac{(n+|m|+2)!}{(n-|m|)!} - \sum_{m=-n}^{-1} c_{n}^{*} c_{n+1}^{*} g_{n,TE}^{m,*} g_{n+1,TE}^{m+1} \frac{(n+|m|+1)!}{(n-|m|+1)!} - \sum_{m=-n}^{-1} c_{n}^{*} c_{n+1} g_{n,TE}^{m,*} g_{n+1,TE}^{m+1} \frac{(n+|m|)!}{(n-|m|)!} \right\}$$

$$(13)$$

$$C_{n}^{m} = \frac{2n+1}{[n(n+1)]^{2}} d_{n} c_{n}^{*} \times \{ \sum_{m=0}^{n} (g_{n,TM}^{m+1} g_{n,TE}^{m,*} \pm g_{n,TM}^{m} g_{n,TE}^{m+1,*}) \frac{(n+|m|+1)!}{(n-|m|-1)!} - \sum_{m=-n}^{-1} (g_{n,TM}^{m+1} g_{n,TE}^{m,*} \pm g_{n,TM}^{m} g_{n,TE}^{m+1,*}) \frac{(n+|m|)!}{(n-|m|)!} \}$$

$$(14)$$

181 
$$D_n^m = \frac{1}{(n+1)^2} d_n^* d_{n+1} g_{n,TM}^{m,*} g_{n+1,TM}^m \frac{(n+|m|+1)!}{(n-|m|)!}$$
 (15)

182 
$$E_n^m = \frac{1}{(n+1)^2} c_n^* c_{n+1} g_{n,TE}^{m,*} g_{n+1,TE}^m \frac{(n+|m|+1)!}{(n-|m|)!}$$
 (16)

183 
$$F_n^m = m \frac{2n+1}{[n(n+1)]^2} c_n^* d_n g_{n,TE}^{m,*} g_{n,TM}^m \frac{(n+|m|)!}{(n-|m|)!}$$
(17)

where  $g_{n,TE}^m$  and  $g_{n,TM}^m$  are the beam shape coefficients (BSCs) of the GLMT which encode the

structure of the illuminating laser beam. Please note that Eqs. (10)-(17) here are slightly

different from those given in Ref. [22] since the conventional form of the scattering coefficients

187  $c_n, d_n$  in the classical Lorenz-Mie theory [27-29] for non-magnetic spheres were used here:

$$c_{n} = \frac{M \left[ \psi_{n}(x) \xi_{n}'(x) - \xi_{n}(x) \psi_{n}'(x) \right]}{\psi_{n}(m_{p}x) \xi_{n}'(x) - M \xi_{n}(x) \psi_{n}'(m_{p}x)}$$

$$d_{n} = \frac{M \left[ \psi_{n}(x) \xi_{n}'(x) - \xi_{n}(x) \psi_{n}'(x) \right]}{M \psi_{n}(m_{p}x) \xi_{n}'(x) - \xi_{n}(x) \psi_{n}'(m_{p}x)}$$
(18)

While the scattering coefficients  $c_n, d_n$  in Ref. [22] are valid for arbitrary refractive index.

190 Furthermore,

191

$$R_{n} = \frac{\operatorname{Im}\left[m_{p}\psi_{n+1}\left(m_{p}x\right)\cdot\psi_{n}^{*}\left(m_{p}x\right)\right]}{\operatorname{Im}\left(m_{p}^{2}\right)}$$

$$S_{n} = -\frac{i}{2\operatorname{Im}\left(m_{p}^{2}\right)}\begin{bmatrix} x\left(m_{p}\left|\psi_{n}\left(m_{p}x\right)\right|^{2} + m_{p}^{*}\left|\psi_{n+1}\left(m_{p}x\right)\right|^{2}\right) \\ -\left(m_{p}^{2} + 2(n+1)\frac{\operatorname{Re}(m_{p}^{2})}{m_{p}}\right)R_{n} + (2n+1)m_{p}^{*}R_{n+1} \end{bmatrix}$$
(19)

192193 To simplify the numerical implementation, the followings are introduced [7]:

194 
$$R_{n} = \frac{R_{n}}{|\psi(m_{p}x)|^{2}} = \frac{\text{Im}(m_{p}C_{n})}{\text{Im}(m_{p}^{2})}$$
 (20)

195 
$$S_{n} = \frac{S_{n}}{|\psi(m_{p}x)|^{2}} = \frac{-i}{2\operatorname{Im}(m_{p}^{2})} \begin{cases} x(m_{p} + m_{p}^{*} | C_{n} |^{2}) \\ -\left[m_{p} + 2(n+1)\frac{\operatorname{Re}(m_{p}^{2})}{m_{p}}\right] R_{n} + (2n+1)m_{p}^{*} | C_{n} |^{2} R_{n+1} \end{cases}$$
(21)

196 where

197 
$$C_n = \frac{\psi_{n+1}(m_p x)}{\psi_n(m_p x)} = \frac{n+1}{m_p x} - D_n$$
 (22)

198 
$$c_{n} = \psi_{n}(m_{p}x)c_{n}; d_{n} = \psi_{n}(m_{p}x)d_{n}$$
 (23)

199 Thus, we have:

200 
$$J_{z} = -\frac{12nk}{|m_{p}|^{2} x^{3}} \operatorname{Im} \sum_{n=1}^{\infty} \sum_{m=-n}^{n} \left[ D_{n}^{m} \left( \frac{S_{n}^{*}}{C_{n}} + \frac{n+1}{m_{p}} R_{n+1} C_{n}^{*} \right) + E_{n}^{m} \left( -\frac{S_{n}}{C_{n}} + \frac{n+1}{m_{p}} \frac{R_{n}}{C_{n}} \right) + i F_{n}^{m} S_{n} \right] (24)$$

$$J_{\left\{\frac{x}{y}\right\}} = \frac{6nk}{|m_{p}|^{2} x^{3}} \left\{\frac{1m}{Re}\right\} \sum_{n=1}^{\infty} \sum_{m=-n}^{n} \left[A_{n,1}^{m} \left(\frac{S_{n}^{*}}{C_{n}} + \frac{n+1}{m_{p}} R_{n+1} C_{n}^{*}\right) + B_{n,1}^{m} \left(-\frac{S_{n}}{C_{n}} + \frac{n+1}{m_{p}} \frac{R_{n}}{C_{n}}\right) + A_{n,2}^{m} \left(\frac{S_{n}^{*}}{C_{n}^{*}} + \frac{n+1}{m_{p}} R_{n+1} C_{n}\right) + B_{n,2}^{m} \left(-\frac{S_{n}}{C_{n}^{*}} + \frac{n+1}{m_{p}} \frac{R_{n}}{C_{n}^{*}}\right) + iC_{n}^{m} S_{n}\right]$$

$$(25)$$

$$A_{n,1}^{m} = \frac{1}{(n+1)^{2}} d_{n}^{*} d_{n+1} \left\{ \sum_{m=0}^{n} g_{n,TM}^{m,*} g_{n+1,TM}^{m+1} \frac{(n+|m|+2)!}{(n-|m|)!} - \sum_{m=-n}^{-1} g_{n,TM}^{m,*} g_{n+1,TM}^{m+1} \frac{(n+|m|)!}{(n-|m|)!} \right\}$$

$$A_{n,2}^{m} = \frac{1}{(n+1)^{2}} d_{n} d_{n+1}^{*} \left\{ \sum_{m=0}^{n-1} g_{n+1,TM}^{m,*} g_{n,TM}^{m+1} \frac{(n+|m|+1)!}{(n-|m|+1)!} - \sum_{m=-n-1}^{-1} g_{n+1,TM}^{m,*} g_{n,TM}^{m+1} \frac{(n+|m|+1)!}{(n-|m|+1)!} \right\}$$

$$(26)$$

$$B_{n,1}^{m} = \frac{1}{(n+1)^{2}} c_{n}^{*} c_{n+1} \left\{ \sum_{m=0}^{n} g_{n,TE}^{m,*} g_{n+1,TE}^{m+1} \frac{(n+|m|+2)!}{(n-|m|)!} - \sum_{m=-n}^{-1} g_{n,TE}^{m,*} g_{n+1,TE}^{m+1} \frac{(n+|m|)!}{(n-|m|)!} \right\}$$

$$B_{n,2}^{m} = \frac{1}{(n+1)^{2}} c_{n} c_{n+1}^{*} \left\{ \sum_{m=0}^{n-1} g_{n+1,TE}^{m,*} g_{n,TE}^{m+1} \frac{(n+|m|+1)!}{(n-|m|-1)!} - \sum_{m=-n-1}^{-1} g_{n+1,TE}^{m,*} g_{n,TE}^{m+1} \frac{(n+|m|+1)!}{(n-|m|+1)!} \right\}$$

$$(27)$$

$$C_{n}^{m} = \frac{2n+1}{[n(n+1)]^{2}} d_{n} c_{n}^{*} \times \{ \sum_{m=0}^{n} (g_{n,TM}^{m+1} g_{n,TE}^{m,*} \pm g_{n,TM}^{m} g_{n,TE}^{m+1,*}) \frac{(n+|m|+1)!}{(n-|m|-1)!} - \sum_{m=-n}^{-1} (g_{n,TM}^{m+1} g_{n,TE}^{m,*} \pm g_{n,TM}^{m} g_{n,TE}^{m+1,*}) \frac{(n+|m|)!}{(n-|m|)!} \}$$

$$(28)$$

$$D_n^m = \frac{1}{(n+1)^2} d_n^* d_{n+1} g_{n,TM}^{m,*} g_{n+1,TM}^m \frac{(n+|m|+1)!}{(n-|m|)!}$$
(29)

$$E_n^m = \frac{1}{(n+1)^2} c_n^* c_{n+1} g_{n,TE}^{m,*} g_{n+1,TE}^m \frac{(n+|m|+1)!}{(n-|m|)!}$$
(30)

$$F_n^m = m \frac{2n+1}{[n(n+1)]^2} c_n^* d_n g_{n,TE}^{m,*} g_{n,TM}^m \frac{(n+|m|)!}{(n-|m|)!}$$
(31)

- Eqs. (24)-(31) can be implemented numerically, once the BSCs of the incident structured beam are known.
- Detailed descriptions of vector circularly symmetric Bessel beams can be found in [30-32].

  A rigorous and efficient approach was given in Ref. [33] for the calculation of BSCs of a
- 212 circularly symmetric Bessel beam, which can be implemented using an angular spectrum
- decomposition (ASD) [34, 35] or any other more conventional methods in the framework of
- 214 GLMT. Analytical expressions of BSCs for x-polarized circularly symmetric Bessel beam can
- be obtained from Ref. [33]:

$$g_{n,\text{TM}}^{m} = -g(\alpha_{0})(-1)^{\frac{m-|m|}{2}} \frac{(n-m)!}{(n+|m|)!} e^{-ik_{z}z_{0}} \left\{ i^{l-m+1}e^{i(l-m+1)\phi_{0}} J_{l-m+1}(\sigma_{0}) \left[ \tau_{n}^{m}(\cos\alpha_{0}) + m\pi_{n}^{m}(\cos\alpha_{0}) \right] + i^{l-m-1}e^{i(l-m-1)\phi_{0}} J_{l-m-1}(\sigma_{0}) \left[ \tau_{n}^{m}(\cos\alpha_{0}) - m\pi_{n}^{m}(\cos\alpha_{0}) \right] \right\}$$

$$g_{n,\text{TE}}^{m} = ig(\alpha_{0})(-1)^{\frac{m-|m|}{2}} \frac{(n-m)!}{(n+|m|)!} e^{-ik_{z}z_{0}} \left\{ i^{l-m+1}e^{i(l-m+1)\phi_{0}} J_{l-m+1}(\sigma_{0}) \left[ \tau_{n}^{m}(\cos\alpha_{0}) + m\pi_{n}^{m}(\cos\alpha_{0}) \right] - i^{l-m-1}e^{i(l-m-1)\phi_{0}} J_{l-m-1}(\sigma_{0}) \left[ \tau_{n}^{m}(\cos\alpha_{0}) - m\pi_{n}^{m}(\cos\alpha_{0}) \right] \right\}$$

$$(32)$$

217 where the generalized Legendre functions have been introduced

218 
$$\pi_n^m(\cos\alpha_0) = \frac{P_n^m(\cos\alpha_0)}{\sin\alpha_0}, \quad \tau_n^m(\cos\alpha_0) = \frac{dP_n^m(\cos\alpha_0)}{d\alpha_0}.$$
 (33)

- 219 and  $\sigma_0 = k_t \rho_0$ ,  $\rho_0 = \left[ x_0^2 + y_0^2 \right]^{1/2}$ ,  $\phi_0 = \tan^{-1} \left( y_0 / x_0 \right)$ . The transverse and longitudinal
- 220 wavenumbers are  $k_t = k_0 \sin \alpha_0$  and  $k_z = k_0 \cos \alpha_0$ , respectively. The  $J_1(\cdot)$  represents an l-order
- Bessel function of the first kind. The  $\alpha_0$  is the half-cone angle of the Bessel beam. The  $g(\alpha_0)$
- is a generalization factor.
- For an on-axis x-polarized Bessel beam, where  $\rho_0 = 0$  and  $\phi_0 = 0$ , all the BSCs are zero
- except  $m = l \pm 1$ , and the BSCs  $g_{n,\text{TM}}^m$  and  $g_{n,\text{TE}}^m$  satisfy the relationship [33]:

$$g_{n,TM}^{l-1} = -ig_{n,TM}^{l-1}, \quad g_{n,TM}^{l+1} = ig_{n,TE}^{l+1}. \tag{34}$$

- Then we have  $A_n^m = B_n^m = C_n^m = 0$ , which results in  $J_x = J_y = 0$ . Inserting Eq. (34) into Eq.
- 227 (11), we have

$$J_{z} = \frac{-12nk}{|M|^{2}} \operatorname{Im} \sum_{n=1}^{\infty} \left\{ -\frac{1}{(n+1)^{2}} \left( c_{n}^{*} c_{n+1} R_{n} + d_{n}^{*} d_{n+1} R_{n+1} \right) \left( \frac{g_{n,TM}^{l+1,*} g_{n+1,TM}^{l+1}}{(n-|l+1|)!} \frac{(n+|l+1|+1)!}{(n-|l-1|)!} \right) \right\} - \frac{1}{(n+1)^{2}} \left( c_{n}^{*} c_{n+1} S_{n} - d_{n}^{*} d_{n+1} S_{n}^{*} \right) \left( \frac{g_{n,TM}^{l+1,*} g_{n+1,TM}^{l+1}}{(n-|l+1|)!} \frac{(n+|l+1|+1)!}{(n-|l+1|)!} \right) - \frac{2n+1}{[n(n+1)]^{2}} c_{n}^{*} d_{n} S_{n} \left[ (l+1) g_{n,TM}^{l+1,*} g_{n,TM}^{l+1} \frac{(n+|l+1|+1)!}{(n-|l+1|)!} - (l-1) g_{n,TM}^{l-1,*} g_{n,TM}^{l-1} \frac{(n+|l+1|)!}{(n-|l+1|)!} \right] \right\}$$

$$(35)$$

which is the same as that given in Ref. [21]. Please note that a factor  $1/2\pi$  is missing in Ref.

230 [21] due to a typo. Specifically, for a zeroth-order Bessel beam l = 0, the BSCs satisfy:

231 
$$g_{n,TM}^{1} = g_{n,TM}^{-1} = -ig_{n,TE}^{-1} = ig_{n,TE}^{1} = \frac{g_{n}}{2},$$
 (36)

- Eq. (35) then reduces to that given by Ambrosio in Ref. [10] considering that a time dependence
- exp( $i\omega t$ ) was used there. Furthermore, if we set  $\alpha = 0^{\circ}$ , the x-polarized Bessel beam reduces to
- the case of a plane wave, where  $g_n = 1.0$ , then Eq. (35) reduces to that given by Mackowski
- in Ref. [7] for a plane wave illumination.
- Using the approach given in Ref. [33], the BSCs of a TM polarized circularly symmetric
- Bessel beam with its beam center located at an arbitrary point  $(x_0, y_0, z_0)$  are:

238 
$$g_{n,\text{TM}}^{m,(\text{TM mode})} = -g\left(\alpha\right)(-1)^{\frac{m-|m|}{2}} \frac{(n-m)!}{(n+|m|)!} e^{-ik_z z_0} J_{m-l}(k_\rho \rho_0) e^{i(l-m)\phi_0} i^{l-m} \tau_n^m(\cos \alpha)$$
(37)

239 
$$g_{n,\text{TE}}^{m,(\text{TM mode})} = g(\alpha)(-1)^{\frac{m-|m|}{2}} \frac{(n-m)!}{(n+|m|)!} e^{-ik_z z_0} i^{l-m-1} J_{m-l}(k_\rho \rho_0) e^{i(l-m)\phi_0} m \pi_n^m(\cos \alpha)$$
(38)

- 240 where the superscript "TM mode" indicates the TM-polarization. Considering the relationship
- between the electromagnetic field of *TM*-polarization and that of *TE*-polarization:

242 
$$\mathbf{E}^{\text{TE mode}} / E_0 = \mathbf{B}^{\text{TM mode}} / B_0, \quad \mathbf{B}^{\text{TE mode}} / B_0 = -\mathbf{E}^{\text{TM mode}} / E_0. \tag{39}$$

243 we have

$$\begin{cases}
g_{n,\text{TM}}^{m,(\text{TE mode})} \\
g_{n,\text{TE}}^{m,(\text{TE mode})}
\end{cases} = \begin{cases}
g_{n,\text{TE}}^{m,(\text{TM mode})} \\
-g_{n,\text{TM}}^{m,(\text{TM mode})}
\end{cases}$$
(40)

- where the superscript "TE mode" indicates the TE-polarization. For beam order l = 0, the zero-
- order Bessel beam in the TM mode and that in the TE mode is also known as radially polarized
- and azimuthally polarized, respectively.
- For an on-axis *TM*-polarization or *TE*-polarization Bessel beam, where  $\rho_0 = 0$  and  $\phi_0 = 0$ ,
- 249 all the BSCs are zero except m = l, we have:

$$g_{n,\text{TM}}^{l,(\text{TM mode})} = -g\left(\alpha\right) \frac{(n-l)!}{\left(n+|l|\right)!} e^{-ik_z z_0} \tau_n^l(\cos\alpha) \tag{41}$$

$$g_{n,\text{TE}}^{l,(\text{TM mode})} = ig\left(\alpha\right) \frac{(n-l)!}{\left(n+|l|\right)!} e^{-ik_z z_0} l \pi_n^l(\cos\alpha) \tag{42}$$

- Then we have  $A_n^m = B_n^m = C_n^m = 0$ , which results in  $J_x = J_y = 0$ . Inserting Eq. (41)-(42) into
- Eq. (11), the double summary reduces to a single summary of the series as:

254 
$$J_{z} = -\frac{12nk}{|M|^{2} x^{3}} \operatorname{Im} \sum_{n=1}^{\infty} \left[ D_{n}^{l} (S_{n}^{*} + \frac{n+1}{M} R_{n+1}) + E_{n}^{l} (-S_{n} + \frac{n+1}{M} R_{n}) + i F_{n}^{l} S_{n} \right]$$
(43)

#### 3. Numerical results and discussions

255

256

257

258

259

260 261

262

263

264

265

266

267268

269

270

271

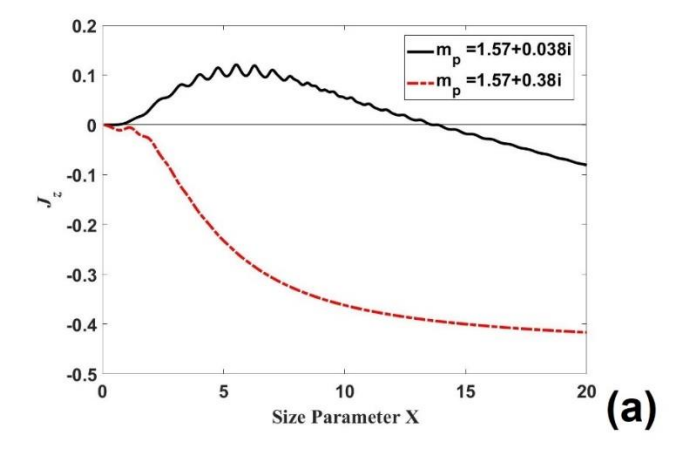
272

273274

Based on the theoretical derivations given in Section 2, a program was written in Fortran 90 to calculate each component of the asymmetry vector of a sphere illuminated by a circularly symmetric Bessel beam. To validate the correctness of our home-built code, the asymmetry factor J<sub>z</sub> was calculated and displayed in Fig. 2(a) for a plane wave illumination. The curves in Fig. 2(a) are reproductions of those of Fig. 1, Fig. 2 in Ref. [7]. Perfect agreements between our results and those in Ref. [7] were achieved as expected since the plane wave illumination is a special case of Bessel beam illumination. Furthermore, ratio of photophoretic force to the weight of a glyceryl particle illuminated by a plane wave was calculated and displayed in Fig. 2(b). The parameters of the ambient atmospheric conditions and those of particles used in the simulations are listed in Table 1, which are the same as those given in the experiment implemented by Arnold and Lewitters [36]. Two kinds of complex refractive indices of the particle are considered, say  $m_p = 1.57 + 0.0475i$  and  $m_p = 1.57 + 0.38i$ , which correspond to the wavelength of  $\lambda$ =10.63 $\mu$ m and  $\lambda$ =9.58 $\mu$ m, respectively. As shown in Fig. 2(b), satisfactory agreements have been achieved between our results and those obtained by Mackowski [7], and the discrepancy is believed to results from certain differences in the thermal and hydrodynamic parameters used in the simulations. The agreements partially indicate the correctness of our theoretical derivations and our home-built code.

Table 1. Parameters of the ambient atmospheric conditions and those of particles used in the simulations

Particle density $\rho_s$	$1.2613 \times 10^3 \mathrm{kg}/\mathrm{m}^3$	Temperature $T_0$	300K
Gas Viscosity $\eta_g$	1.82×10⁻⁵ Pa⋅s	Light Intensity $I_{\lambda}$	$3.8\times10^3\mathrm{W}/\mathrm{m}^2$
Thermal conduction coefficient $k_s$	0.28W/(m·K)	Pressure p	30Torr
Gas constant R	8.31	Mole mass of gas M	28.952 kg/mol



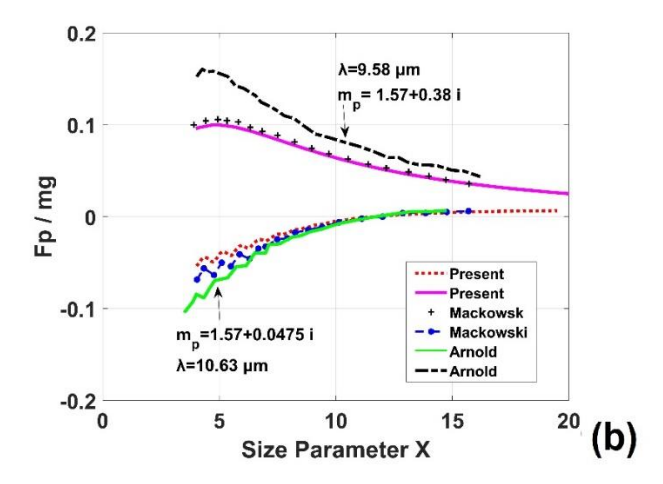


Fig. 2.(a) photophoretic asymmetry factor  $J_z$ , which are reproductions of Fig. 1 and Fig. 2 in Ref. [7], and (b) ratio of photophoretic force to the weight of a glyceryl particle illuminated by a plane wave.

### 3.1 On-axis cases

For the on-axis case, only  $J_z$  is not zero, since we have  $A_n^m = B_n^m = C_n^m = 0$ , which results in  $J_x = J_y = 0$ . The  $J_z$  spectra ( $J_z$  versus the particle size parameter  $x = 2\pi R/\lambda$ ) of a homogeneous sphere with different refractive indices illuminated by a zero-order Bessel beam of radial polarization and of azimuthal polarization are displayed in Fig. 3 and Fig. 4, respectively. Three different half-cone angles of Bessel beams are considered in the simulations to analyze the influence of half-cone angle on the  $J_z$  spectra.

As we can see from Fig. 3 and Fig. 4, the imaginary part of the refractive index plays a significant role in the behaviors of  $J_z$  spectra. For the cases under study, for particles with small absorptivity, for instance  $\kappa = 0.01$  and  $\kappa = 0.038$ , we can observe positive  $J_z$  and thus negative photophoretic force for particles in a large range of size parameter. This range depends on the values of the half-cone angle and of the imaginary part of the refractive index. Generally speaking, the smaller the half-cone angle and the imaginary part of the refractive index, the

larger the size range for positive  $J_z$ . However, when the particle is highly absorbing, for instance  $\kappa = 0.38$  and  $\kappa = 1.0$ , the size range for positive  $J_z$  is very limited and is not so sensitive to the change of the imaginary part of the refractive index or of the half-cone angle.

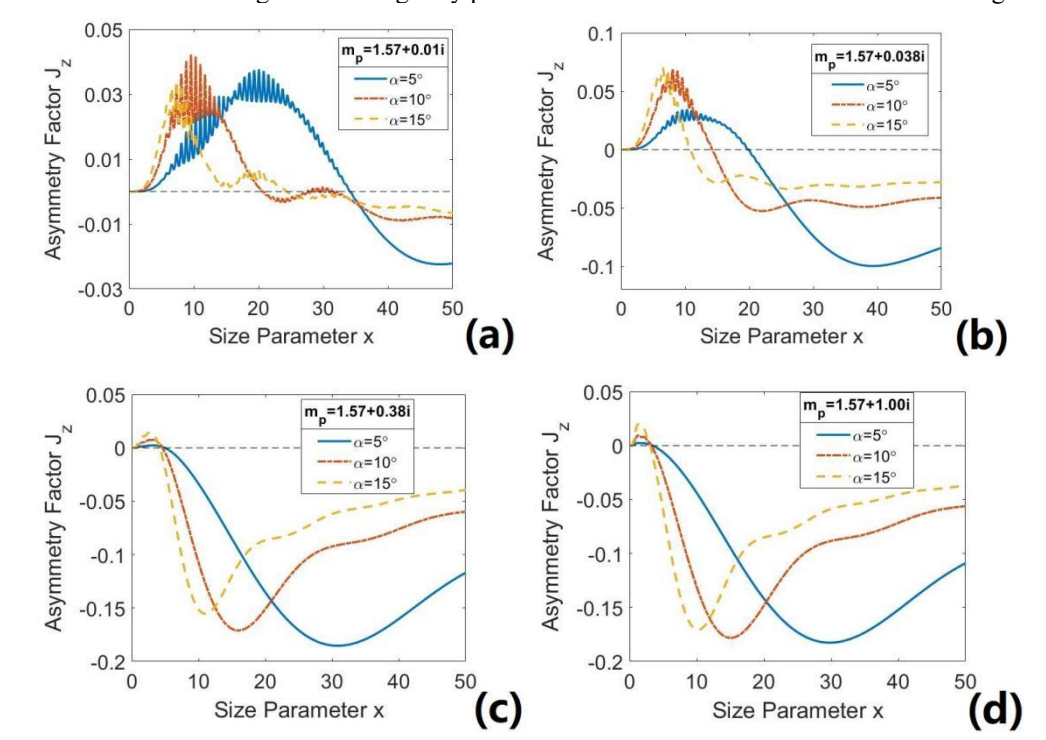


Fig. 3.  $J_z$  spectra for particles with different refractive indices in the case of a zero-order Bessel beam with different half-cone angles. (a)  $m_p = 1.57 + 0.01i$ ; (b)  $m_p = 1.57 + 0.038i$ ; (c)  $m_p = 1.57 + 0.38i$ ; (d)  $m_p = 1.57 + 1.0i$ . The Bessel beam is radially polarized.

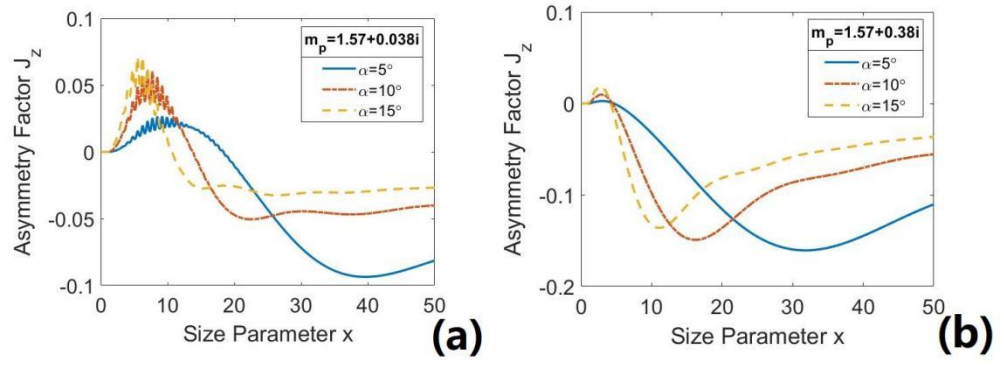


Fig. 4.  $J_z$  spectra for particles with different refractive indices in the case of a zero-order Bessel beam with different half-cone angles. (a)  $m_p = 1.57 + 0.038i$ ; (b)  $m_p = 1.57 + 0.38i$ ; The Bessel beam is azimuthally polarized.

When the imaginary part of the complex refractive index is relatively small, ripple structures can be observed in  $J_z$  for small size parameter, indicating a strong oscillation of the photophoretic force with the change of size parameter. This ripple structure fades away when the imaginary part of the complex refractive index increases or when the size parameter is large.

This ripple structure is believed to be related to the resonant modes in a weekly absorbing sphere, similarly to the ripple structures existing in extinction, scattering and absorption spectra.

As shown in Fig.3c and Fig.3d, when the imaginary part of the complex refractive index is relatively large,  $J_z$  spectra have similar profiles. The similarity between the profiles is because most of the incident light will be absorbed on the illuminated surface of the particle due to high absorptivity. Furthermore, an extreme minimum value of  $J_z$  can be found, which depends on the axicon angle, for instance, the extrema for both curves are around size parameters x = 30 for axicon angle equal to  $5^\circ$ . It is interesting to find that positive  $J_z$  can also be found for high-absorbing particles when the particle is illuminated by a radially or azimuthally polarized Bessel beam. However, only negative  $J_z$  can be found in the case of x-polarized zero-order Bessel beam, as shown in Fig. 3(c)-(d) in [21].

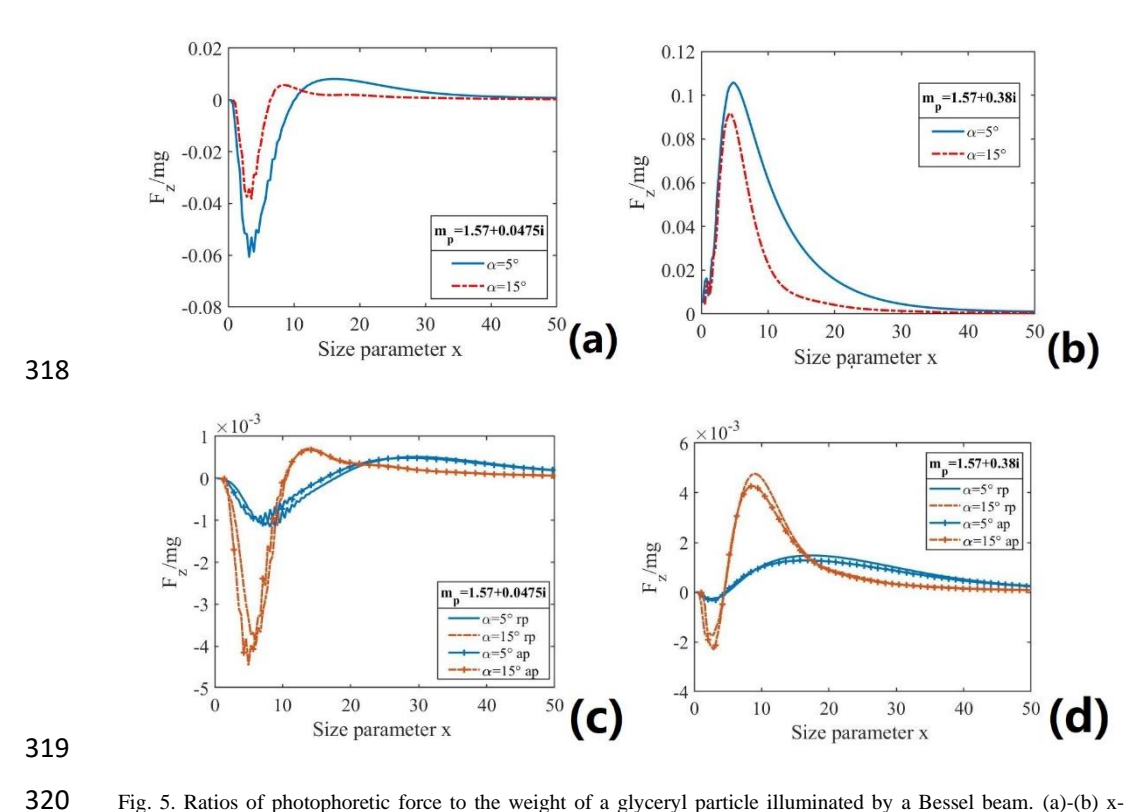


Fig. 5. Ratios of photophoretic force to the weight of a glyceryl particle illuminated by a Bessel beam. (a)-(b) x-polarization; (c)-(d) radial polarization (rp) and azimuthal polarization (ap). Parameters of the ambient atmospheric conditions are the same as those listed in Table 1.

Making a comparison between Fig. 3 and Fig. 4, when the imaginary part of refractive index is the same, we can see that the  $J_z$  spectra pattern are slightly changed when the polarization varies from radial polarization to azimuthal polarization for the cases under study, although we should be aware that the absolute value of  $J_z$  depends on the polarization, resulting in a change of photophoretic force if the polarization is shifted. Ratios of longitudinal photophoretic force  $F_z$  to weight of a glyceryl particle illuminated by a Bessel beam have been calculated and

displayed in Fig. 5 for different polarizations. Two kinds of refractive indices of the particle  $m_p = 1.57 + 0.0475i$  and  $m_p = 1.57 + 0.38i$  have been considered, which correspond to the wavelength of  $\lambda = 10.63 \,\mu\text{m}$  and  $\lambda = 9.58 \,\mu\text{m}$ , respectively. Parameters of the ambient atmosphere conditions are the same as those listed in Table 1.

Ignoring the ripple structure in the spectra, one extreme maximum and one extreme minimum can be observed in all the subfigures of Fig. 5, the corresponding size parameters depending on the value of the imaginary part of the refractive index and on the half-cone angle. As shown in Figs. 5(c) and (d), the spectra profiles of ratios of photophoretic force to the weight are quite similar for the radial polarization and the azimuthal polarization, although the internal field distributions inside of the sphere are quite different [37] in these two polarizations. It indicates that the longitudinal component of the asymmetry vector and the photophoretic force are mainly determined by the intensity profile of the incident beam in the case of a sphere illuminated by a circularly symmetric Bessel beam.

#### 3.2 Off-axis cases

 For the off-axis case, the photophoretic force has both a longitudinal and transverse component. The transverse component can be used to trap the particle inside the beam laterally, whereas the longitudinal component can be used to counterbalance the weight of particles.  $J_x$  spectra and  $J_z$  spectra (J versus the particle size parameter  $x = 2\pi R/\lambda$ ) of a homogeneous sphere with different refractive indices illuminated by an off-axis zero-order Bessel beam are displayed in Fig. 6. Both radial polarization and x-polarization are considered.

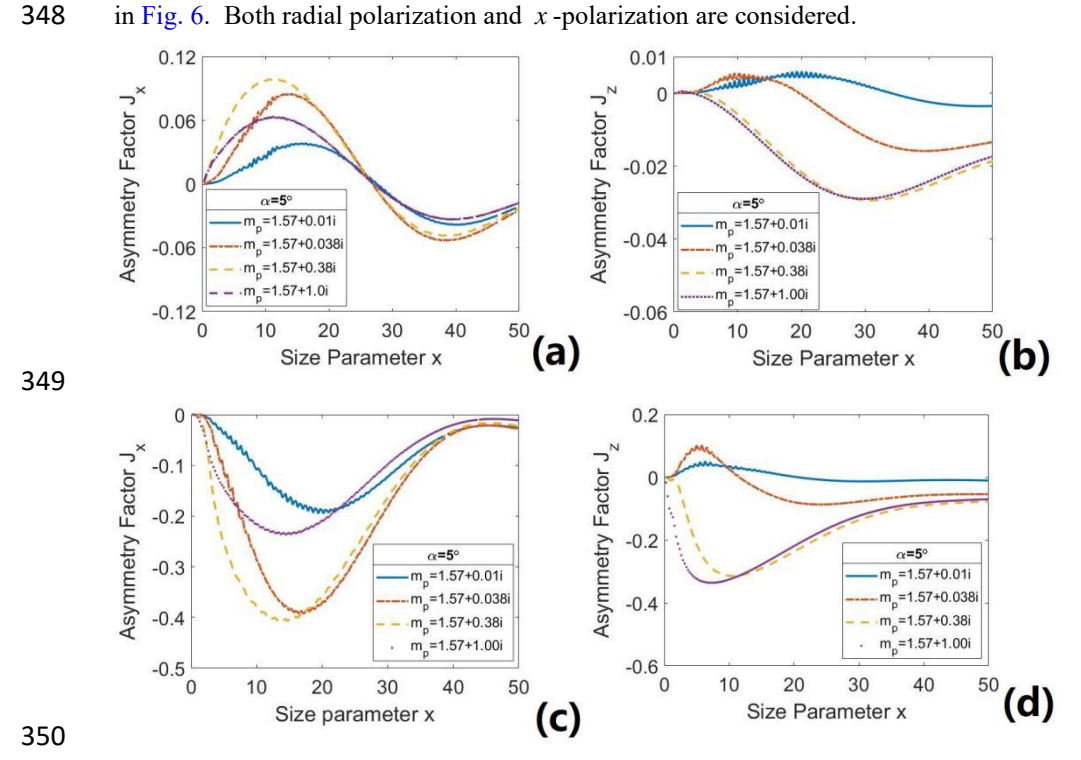


Fig. 6.  $J_x$  spectra and  $J_z$  spectra for different values of the imaginary part of refractive index. The particle is illuminated by an off-axis Bessel beam with beam center located at  $X_0 = 2.5 \mu m$ . (a)-(b) radial polarization, (c)-(d) x-polarization.

351

352

353

354

355

356

357

358

359

360

361

362

363

364

365

366 367

368

369

373

As shown in Fig. 6, ripple structures can be observed in both  $J_x$  spectra and  $J_z$  spectra for particles with small absorptivity. This ripple structure starts to disappear for particles with large size parameter and strong absorptivity. Similar to the cases of on-axis illumination, positive  $J_z$  can be obtained when the absorption is small for both radial polarization and xpolarization, but only negative  $J_z$  exist for particles with strong absorption. As shown in Fig. 6(a), when a Bessel beam of radial polarization is assumed, the  $J_x$  is positive for small size parameters, indicating a restoring photophoretic force is exerted on the particle toward the beam center when the particle moves away from the beam center. This force increases with the increase of the particle size parameter during which positive part of the first lobe of the Bessel beam is covered by the particle step by step. Then  $J_x$  decreases and changes its sign from positive to negative when the particle is too large so that the first lobe of the Bessel beam was totally covered by the particle, and the photophoretic force starts to push the particle away from the beam center. However, when a Bessel beam of x-polarization is applied, as shown in Fig. 6(b), only negative  $J_z$  exist due to the fact that the maximum intensity is located at the beam center, so that the transverse photophoretic force will push the particle away from the beam center.

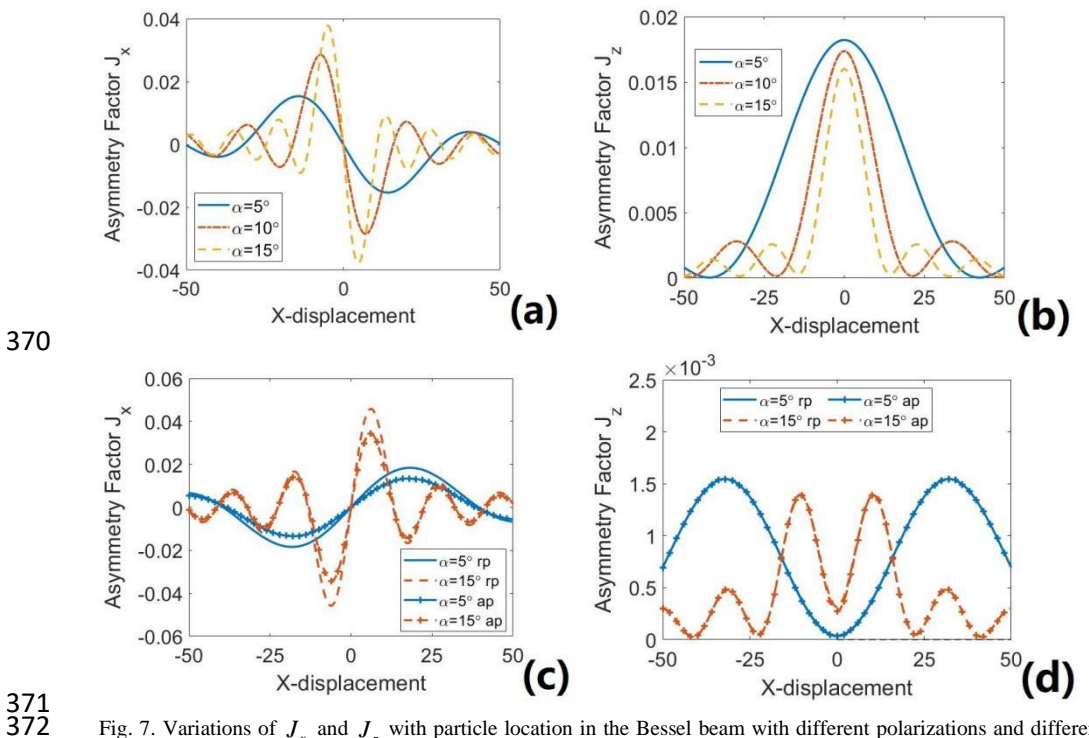


Fig. 7. Variations of  $J_x$  and  $J_z$  with particle location in the Bessel beam with different polarizations and different half-cone angles. (a)-(b) x-polarization; (c)-(d) radial polarization and azimuthal polarization. The radius of the

374

375

376

377

378

379

380

381

382

383

384

385

386

387

388

389

390

391

392

393

394

395

396

397

398

399400

401

402

403

404

405

To analyze the influence of particle locations on the photophoretic force, variations of  $J_x$  and  $J_z$  are predicted and displayed in Fig. 7 with the change of particle locations in the Bessel beam for different polarizations, including x-polarization, radial polarization, and azimuthal polarization. As shown in Fig. 7, all the  $J_z$  patterns are symmetric due to the circularly symmetric characteristics of Bessel beams. There is little difference in the  $J_z$  patterns between the radial polarization and azimuthal polarization. But the difference between the  $J_z$  profile of x -polarization and that of radial polarization is huge. As shown in Fig. 7(b), a maximum of  $J_z$ can be found when the particle sits at the center of the Bessel beam of x-polarization. The  $J_z$ decreases as the particle moves along x-axis away from the beam center. For the radial polarization and azimuthal polarization, the  $J_{\perp}$  has a minimum at the center of beam and then increases as the particle moves away from the beam center, as displayed in Fig. 7(d). The variations of  $J_z$  are similar to the variations of the transverse intensity profile of a Bessel beam, recalling that there is a maximum in the center of a Bessel beam of x-polarization, while a hollow center exists in the spatial intensity distribution of Bessel beam of radial polarization. It is also important to notice that the maximum value of  $J_z$  in x-polarization is around ten times larger than that in radial polarization.

The  $J_x$  profiles are antisymmetric with respect to  $J_x = 0$  when the particle is located at the beam center. The  $J_x$  oscillates periodically as the particle moves transversely along X-axis, the period depends on the half-cone angle reflecting the transverse intensity distribution of the Bessel beam. Although there is little difference in the  $J_z$  patterns between the radial polarization and the azimuthal polarization, and that the  $J_x$  patterns for these two polarizations are similar, the amplitudes of  $J_x$  are different, indicating a different transverse trapping efficiency on particles by different polarizations.

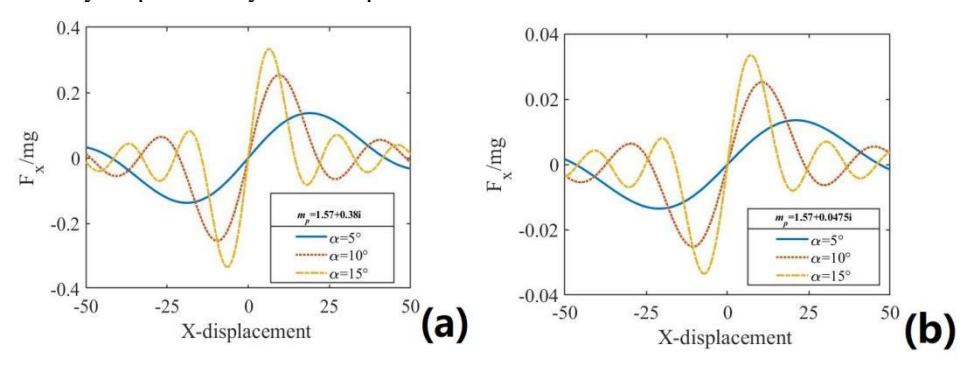


Fig. 8. Ratios of transverse component  $F_x$  of photophoretic force to the weight of a glyceryl particle illuminated by an off-axis Bessel beam of x-polarization. The radius of the particle is  $2.5 \mu m$ .

To provide some references on the trapping efficiency of transverse component of photophoretic force, ratios of transverse component  $F_x$  of photophoretic force to the weight of a glyceryl particle have been calculated and displayed in Fig. 8 for x-polarization. Parameters of the ambient atmosphere conditions are the same as those listed in Table 1. As shown in Fig.

- 8, the imaginary part of refractive index has no influence on the ratio profile as the particle
- 407 moves transversely. However, it plays a significant role on the absolute value of photophoretic
- 408 force. The ratio of photophoretic force to weight can be different as high as ten times for a
- glyceryl particle with  $m_n = 1.57 + 0.0475i$  and that with  $m_n = 1.57 + 0.38i$ . Similar behaviors
- being valid for radial polarization and azimuthal polarization, the results are not displayed.

#### 4. Conclusions

411

412

413

414

415

416

417

418

419

420

421

422

423

424

425

426

427

428

429

430

431

432 433

434

436

In this paper, longitudinal and transverse photophoretic forces on a homogeneous sphere exerted by a zero-order Bessel beam with selective polarization are analyzed. The influences of particle size, absorptivity of the particle, half-cone angle and polarizations of the Bessel beam, and particle location in the laser beam on the asymmetry vector and on the photophoretic force are explored. The results show that ripple structures exist in both J, spectra and J. spectra for particles with small absorptivity. This ripple structure starts to disappear for particles with large size parameter and strong absorptivity. Due to the circularly symmetric characteristics of Bessel beams, all the  $J_z$  patterns are symmetric and the  $J_z$  patterns are antisymmetric when the particle moves transversely away from the beam center. The J spectra of radial polarization are quite similar to that of azimuthal polarization, although big differences exist in the internal field distribution for these two polarizations, which indicates that the asymmetry vector and the photophoretic force are mainly determined by the intensity profile of the incident beam in the case of a sphere illuminated by a circularly symmetric Bessel beam. But it is worth mentioning that the amplitudes of J are different in different polarizations, indicating a different trapping efficiency on particles. The predicted dynamic behaviors of photophoretic force on the particle influenced by various parameters give important references to the manipulation of particles trapped in a structured beam and provide significant insights into the working mechanism underpinning the development of novel heat-mediated optical manipulation techniques, measurement of the refractive index of particle, and others.

- **Funding.** The Innovation Capability Support Program of Shaanxi (Grant no. 2021JZY-006); Fundamental Research Funds for the Central Universities (Grant no. XJS190507); Foreigner Young Talent Program (Grant no. QN20200027010); National Council for Scientific and Technological Development (CNPq, Brazil) (426990/2018-8,309201/2021-7); São Paulo Research Foundation (FAPESP, Brazil) (2021/06121-0,2020/05280-5).
- **Disclosures.** The authors declare no conflicts of interest.

#### References

- 437 1. Q. Yang, S. L. Neale, and J. H. Marsh, "Microparticle manipulation using laser-induced thermophoresis and thermal convection flow," Sci Rep-Uk **10**(2020).
- 439 2. G. Gouesbet, "Generalized Lorenz-Mie theories and mechanical effects of laser light,
  440 on the occasion of Arthur Ashkin's receipt of the 2018 Nobel prize in physics for his
  441 pioneering work in optical levitation and manipulation: A review," Journal of
  442 Quantitative Spectroscopy and Radiative Transfer 225, 258-277 (2019).
- 443 3. Z. Gong, Y. L. Pan, G. Videen, and C. Wang, "Optical trapping and manipulation of single particles in air: Principles, technical details, and applications," Journal of Quantitative Spectroscopy and Radiative Transfer **214**, 94-119 (2018).
- 4. Z. Y. Gong, Y. L. Pan, and C. J. Wang, "Optical configurations for photophoretic trap of single particles in air," Rev Sci Instrum **87**(2016).
- 5. D. E. Smalley, E. Nygaard, K. Squire, J. Van Wagoner, J. Rasmussen, S. Gneiting, K. Qaderi, J. Goodsell, W. Rogers, M. Lindsey, K. Costner, A. Monk, M. Pearson, B. Haymore, and J. Peatross, "A photophoretic-trap volumetric display," Nature **553**, 486-+ (2018).
- 452 6. H. Horvath, "Photophoresis a Forgotten Force ??," Kona **31**, 181-199 (2014).

- 7. D. W. Mackowski, "Photopheresis of aerosol particles in the free molecular and slip-flow regimes," Int. J. Heat Mass Transfer **32**, 843-854 (1989).
- 455 8. L. A. Ambrosio, "Photophoresis in the slip-flow and free molecular regimes for arbitrary-index particles," Journal of Quantitative Spectroscopy and Radiative Transfer, 107276 (2020).
- 458 9. Y. I. Yalamov, V. B. Kutukov, and E. R. Shchukin, "Theory of the photophoretic motion of the large-size volatile aerosol particle," Journal of Colloid and Interface ence **57**, 460 564–571 (1976).
- 461 10. L. A. Ambrosio, "Longitudinal photophoresis of on-axis axisymmetric beams of the first kind using the generalized Lorenz-Mie theory," Journal of Quantitative Spectroscopy & Radiative Transfer **To be published**(2021).
- 464 11. C. L. Ou and H. J. Keh, "Low-Knudsen-number photophoresis of aerosol spheroids," J Colloid Interf Sci **282**, 69-79 (2005).
- 466 12. W. Zulehner and H. Rohatschek, "Representation and calculation of photophoretic forces and torques," Journal of Aerosol Science **26**, 201-210 (1995).
- 468 13. V. Shvedov, A. R. Davoyan, C. Hnatovsky, N. Engheta, and W. Krolikowski, "A long-range polarization-controlled optical tractor beam," Nat Photonics **8**, 846-850 (2014).
- 470 14. A. S. Desyatnikov, V. G. Shvedov, A. V. Rode, W. Krolikowski, and Y. S. Kivshar, 471 "Photophoretic manipulation of absorbing aerosol particles with vortex beams: 472 theory versus experiment," Optics Express 17, 8201-8211 (2009).
- 473 15. F. Mitri, "Longitudinal and transverse optical scatteringasymmetry parameters for a dielectric cylinder inlight-sheets of arbitrary wavefronts and polarization," Applied Optics **60**, 1678-1685 (2021).
- 476 16. F. G. Mitri, "Longitudinal and transverse PAFs for an absorptive magneto-dielectric circular cylinder in light-sheets of arbitrary wavefronts and polarization," Applied Optics **60**, 7937-7944 (2021).
- 479 17. F. G. Mitri, "Photophoretic asymmetry factors for an absorptive dielectric cylinder near a reflecting planar boundary," J Opt Soc Am A **38**, 1901-1910 (2021).
- 481 18. F. G. Mitri, "Effect of a perfectly conducting corner space on the PAFs for an absorptive dielectric circular cylinder," J Opt Soc Am B **38**, 3910-3919 (2021).
- 483 19. F. G. Mitri, "Lagrangian PAFs in multiple optical scattering by two absorptive dielectric parallel cylinders," Journal of the Optical Society of America B **39**, 742-750 (2022).
- 486 20. L. A. Ambrosio, "Generalized Lorenz-Mie theory in the analysis of longitudinal 487 photophoresis of arbitrary-index particles: On-axis axisymmetric beams of the first 488 kind," Journal of Quantitative Spectroscopy & Radiative Transfer **275**(2021).
- 489 21. H. Wang, J. Wang, W. Dong, Y. Han, L. A. Ambrosio, and L. Liu, "Theoretical prediction of photophoretic force on a dielectric sphere illuminated by a circularly symmetric high-order Bessel beam: on-axis case," Opt Express **29**, 26894-26908 (2021).
- 492 22. L. A. Ambrosio, J. Wang, and G. Gouesbet, "Towards photophoresis with the generalized Lorenz-Mie theory," Journal of Quantitative Spectroscopy & Radiative Transfer **To be pulished**(2022).
- 495 23. V. G. Shvedov, C. Hnatovsky, N. Eckerskorn, A. V. Rode, and W. Krolikowski, 496 "Polarization-sensitive photophoresis," Appl Phys Lett **101**, 156-159 (2012).
- 497 24. L. D. Reed, "Low Knudsen number photophoresis," Journal of Aerosol Science **8**, 123-498 131 (1977).
- 499 25. G. M. Hidy and J. R. Brock, "Photophoresis and the descent of particles into the lower stratosphere," Journal of Geophysical Research **72**, 455-460 (1967).

- A. Sarofim, E. Barziv, J. P. Longwell, R. E. Spjut, and W. M. Greene, "Photophoresis of irradiated spheres: absorption centers," J.opt.soc.am.b **2**, 866-866 (1985).
- 503 27. G. Gouesbet, "T-matrix formulation and generalized Lorenz-Mie theories in spherical coordinates," Opt. Commun. **283**, 517-521 (2010).
- J. Huang, Y. Zhao, H. Yang, J. Wang, P. Briard, and Y. Han, "Characteristics of photonic jets generated by a dielectric sphere illuminated by a Gaussian beam," Applied Optics
   59, 6390-6398 (2020).
- 508 29. G. Gouesbet and G. Gréhan, *Generalized Lorenz-Mie Theories Second Edition* (Springer, Berlin, 2017).
- J. J. Wang, T. Wriedt, J. A. Lock, and L. Madler, "General description of circularly
   symmetric Bessel beams of arbitrary order," Journal of Quantitative Spectroscopy &
   Radiative Transfer 184, 218-232 (2016).
- J. J. Wang, T. Wriedt, J. A. Lock, and Y. C. Jiao, "General description of transverse mode Bessel beams and construction of basis Bessel fields," Journal of Quantitative
   Spectroscopy & Radiative Transfer 195, 8-17 (2017).
- 516 32. F. G. Mitri, R. X. Li, L. X. Guo, and C. Y. Ding, "Resonance scattering of a dielectric sphere illuminated by electromagnetic Bessel non-diffracting (vortex) beams with arbitrary incidence and selective polarizations," Ann Phys-New York **363**, 562-563 (2015).
- J. J. Wang, T. Wriedt, L. Mädler, and Y. P. Han, "Multipole expansion of circularly symmetric Bessel beams of arbitrary order for scattering calculation," Opt. Commun.
   387, 102-109 (2017).
- 523 34. J. Chen, J. Ng, P. Wang, and Z. F. Lin, "Analytical partial wave expansion of vector Bessel beam and its application to optical binding," Optics Letters **35**, 1674-1676; erratum: 1636(1677): 1243-1243 (2010).
- 526 35. F. G. Mitri, R. X. Li, L. X. Guo, and C. Y. Ding, "Optical tractor Bessel polarized beams,"
   527 Journal of Quantitative Spectroscopy & Radiative Transfer 187, 97-115 (2017).
- 528 36. S. Arnold and M. Lewittes, "Size dependence of the photophoretic force," J Appl Phys 529 53, 5314-5319 (1982).
- 530 37. F. Wu, J. J. Wang, Z. Cui, S. Aihoon, P. Briard, and Y. P. Han, "Polarization-sensitive photonic jet of a dielectric sphere excited by a zero-order Bessel beam," Journal of Quantitative Spectroscopy & Radiative Transfer **280**, 108093 (2022).